NASA TN D-1228

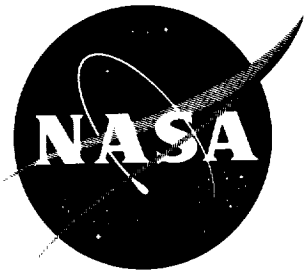

TECHNICAL NOTE

D-1228

INVESTIGATION OF THE STATIC LONGITUDINAL AERODYNAMIC CHARACTERISTICS OF A 1/10-SCALE MODEL OF THE BLUE SCOUT JR. AT MACH NUMBERS FROM 0.40 TO 1.03

By Thomas C. Kelly and Robert J. Keynton

Langley Research Center
Langley Station, Hampton, Va.

NATIONAL AERONAUTICS AND SPACE ADMINISTRATION

WASHINGTON April 1962

NATIONAL AERONAUTICS AND SPACE ADMINISTRATION

TECHNICAL NOTE D-1228

INVESTIGATION OF THE STATIC LONGITUDINAL AERODYNAMIC CHARACTERISTICS OF A 1/10-SCALE MODEL OF THE BLUE SCOUT JR. AT MACH NUMBERS FROM 0.40 TO 1.03

By Thomas C. Kelly and Robert J. Keynton

SUMMARY

Results have been obtained in the Langley 8-foot transonic pressure tunnel at Mach numbers from 0.40 to 1.03 for a 1/10-scale model of the Blue Scout Jr. Tests extended over an angle-of-attack range from about -6° to 6° at a Reynolds number per foot of approximately 4.0×10^{6}.

Results indicated that the complete configuration exhibited nonlinear variations of normal-force and pitching-moment coefficients with angle of attack which were attributed to the downwash field of the forward fins and its effects on the rear fins. The complete configuration was stable about the test center-of-gravity location which was close to the estimated full-scale-vehicle initial center-of-gravity location.

INTRODUCTION

During the design and development of the Scout vehicle, it was realized that with a relatively small effort other vehicles could be developed which could utilize many of the Scout components. One of these vehicles, known popularly as the Blue Scout Jr., was designed for use as a deep space probe with an apogee altitude on the order of 15,000 nautical miles.

As part of the Blue Scout Jr. development program, tests were conducted in the Langley 8-foot transonic pressure tunnel to determine the static longitudinal aerodynamic characteristics of a 1/10-scale model of the Blue Scout Jr. at Mach numbers from 0.40 to 1.03 and at angles of attack from about -6° to 6°. The Reynolds number per foot for the tests was approximately 4.0×10^{6}.

Results of tests of some related Scout configurations are available in references 1 to 3.

SYMBOLS

Aerodynamic force and moment data are referred to the body system of axes. Coefficients are based on an area of 0.0524 square foot and a length of 3.10 inches. Pitching moments are measured about a point located on the model center line at 67.1 percent of the body length.

A	body maximum cross-sectional area, 0.0524 sq ft
C_A	axial-force coefficient, $\frac{\text{Axial force}}{qA}$
$C_{A,b}$	base axial-force coefficient, $\frac{\text{Base axial force}}{qA}$
C_m	pitching-moment coefficient, $\frac{\text{Pitching moment}}{qAd}$
C_{m_α}	pitching-moment-curve slope, $\frac{\partial C_m}{\partial \alpha}$, per deg (measured at $\alpha = 0^\circ$)
C_N	normal-force coefficient, $\frac{\text{Normal force}}{qA}$
C_{N_α}	normal-force-curve slope, $\frac{\partial C_N}{\partial \alpha}$, per deg (measured at $\alpha = 0^\circ$)
D	cylindrical diameter, in.
d	body maximum cylindrical diameter, 3.10 in.
l	model overall length, measured from nose-cone apex to fin trailing edge, in.
M	Mach number
q	free-stream dynamic pressure, lb/sq ft

r radius of curvature, in.

x distance, measured from nose-cone apex, in.

α angle of attack of body center line, deg

Subscript:

cp center of pressure

APPARATUS AND TESTS

Model

Model details and design dimensions are presented in figure 1. The configuration consisted essentially of two sets of delta-planform, cruciform-mounted fins on a staged body of revolution having a fineness ratio of approximately 16. The forward fins, located at the base of the second stage, had a leading-edge sweepback of 70.6° and employed single-wedge streamwise airfoil sections having an included angle of 2.9°. The rear fins, mounted at the base of the first stage, had a leading-edge sweep of 45° and 8° included-angle single-wedge airfoil sections. Model photographs are shown as figure 2.

It should be noted that the 1/10-scale model used for the present investigation was constructed prior to the establishment of the final full-scale-vehicle geometry and, as a result, differed from an exact 1/10-scale model of the full-scale vehicle in several respects. These differences are indicated in figure 3, wherein the test configuration is compared with an early Blue Scout Jr. configuration. The differences consist of slight variations in nose shape and body diameter, in the axial location of the fins relative to the body, and in the included streamwise wedge angle of the second-stage fins. Also, the protruding first-stage rocket nozzle was not simulated on the test model. These differences and their effects should be kept in mind if an attempt is made to compare the present results with full-scale flight results.

Tests and Procedure

Tests were conducted in the Langley 8-foot transonic pressure tunnel over a Mach number range from 0.40 to 1.03 and through an angle-of-attack range from approximately -6° to 6°. Reynolds numbers per foot for the tests were maintained at 3.88×10^6 for a Mach number of 0.40 and 4.12×10^6 for Mach numbers from 0.60 to 1.03.

Four model configurations were tested and are designated the complete configuration, body plus rear fins, body plus forward fins, and body alone.

All tests were conducted with transition fixed. The transition strips, located 1.50 inches from the nose cone apex, were 0.1 inch wide and were composed of No. 60 carborundum grains set in a plastic adhesive.

Corrections

Effects of subsonic boundary interference in the slotted test section were considered negligible and no corrections for these effects have been applied. Also, no test data are presented for Mach numbers at which supersonic boundary-reflected disturbances would be expected to affect the results.

Axial-force data presented herein have been adjusted to correspond to the condition of free-stream static pressure acting at the model base and in the balance chamber.

Accuracy

The estimated accuracies of the measured coefficients, based on instrument calibration and data repeatability, are within the following limits:

	M = 0.40	M = 1.03
C_N	±0.08	±0.04
C_A	±0.017	±0.008
C_m	±0.046	±0.021

Model angle of attack is estimated to be accurate within ±0.1°.

PRESENTATION OF RESULTS

The figures presenting results of this investigation are listed in the following table:

	Figure
Variation of normal-force coefficient with angle of attack	4
Variation of axial-force coefficient with angle of attack	5
Variation of pitching-moment coefficient with angle of attack	6

Figure

In order to facilitate presentation of the data, staggered scales have been used in some of the figures and care should be taken in selecting the proper zero axis for each curve. With regard to the center-of-pressure data presented in figure 7, it should be noted that the flagged test points at an angle of attack of 0° were computed by using C_{m_α} and C_{N_α} which were measured at an angle of attack of approximately 0°.

DISCUSSION

Comparison of normal-force (fig. 4) and pitching-moment (fig. 6) results for the various configurations indicates that the nonlinearities that are evident in the curves for the complete configuration (figs. 4(a) and 6(a)) appear only slightly in the curves for the configurations having only rear fins (figs. 4(b) and 6(b)) or only forward fins (figs. 4(c) and 6(c)), or for the body alone (figs. 4(d) and 6(d)). These results suggest that the nonlinearities are associated with the downwash field of the forward fins and its effects on the rear fins. Because of these downwash effects normal-force-curve slopes for the complete configuration are relatively low at angles of attack near 0° at the higher Mach numbers when compared with the body having only rear fins. (See fig. 8(a).) Comparison of the curves of normal-force coefficient as a function of angle of attack for these two configurations, however, indicates that at the higher angles of attack the complete configuration develops noticeably more normal force (figs. 4(a) and 4(b)), as would be expected.

The variation of center-of-pressure location with Mach number for the four test configurations (fig. 8(a)) indicates only slight variations (± 0.03) over the range of Mach numbers of the investigation. The complete configuration is seen to be stable about the test center-of-gravity location ($x/l = 0.671$) which is close to the estimated full-scale-vehicle initial center-of-gravity location.

An attempt has been made to estimate the normal-force, pitch, and center-of-pressure characteristics for the complete configuration by use of the method of reference 4. The results for Mach numbers of 0.40 and 0.80 are also indicated in figure 8(a). Estimates of normal-force-curve slopes are in good agreement with the experimental results at both Mach numbers. Comparison of the pitching-moment characteristics indicates

fair agreement between experiment and theory at a Mach number of 0.40 and good agreement at a Mach number of 0.80. Center-of-pressure locations are predicted within 3 percent of the body length at both Mach numbers.

Axial-force results, summarized in figure 8(b), indicate effects which are qualitatively similar to those noted in reference 1 for the 1/10-scale three-stage Scout model. Addition of the forward fins is seen to have negligible effects on the base axial force. Further addition of the main rear fins causes sizeable increases in base axial force and in the transonic drag rise.

CONCLUDING REMARKS

Results of an investigation of the static longitudinal aerodynamic characteristics of a 1/10-scale model of the Blue Scout Jr. at Mach numbers from 0.40 to 1.03 have indicated that the complete configuration exhibited nonlinear variations of normal-force and pitching-moment coefficients with angle of attack which were attributed to the downwash field of the forward fins and its effect on the rear fins and that the complete configuration was stable about the test center-of-gravity location which was close to the estimated full-scale-vehicle initial center-of-gravity location.

Langley Research Center,
National Aeronautics and Space Administration,
Langley Air Force Base, Va., January 17, 1962.

REFERENCES

1. Kelly, Thomas C.: Transonic Wind-Tunnel Investigation of the Static Longitudinal Aerodynamic Characteristics of Several Configurations of the Scout Vehicle and of a Number of Related Models. NASA TN D-794, 1961.

2. Kelly, Thomas C.: Aerodynamic Loading Characteristics at Mach Numbers From 0.80 to 1.20 of a 1/10-Scale Three-Stage Scout Model. NASA TN D-945, 1961.

3. Jernell, Lloyd S.: Investigation of the Static Longitudinal and Lateral Stability Characteristics of a 0.10-Scale Model of a Three-Stage Configuration of the Scout Research Vehicle at Mach Numbers of 2.29, 2.96, 3.96, and 4.65. NASA TN D-711, 1961.

4. Pitts, William C., Nielsen, Jack N., and Kaattari, George E.: Lift and Center of Pressure of Wing-Body-Tail Combinations at Subsonic, Transonic, and Supersonic Speeds. NACA Rep. 1307, 1957.

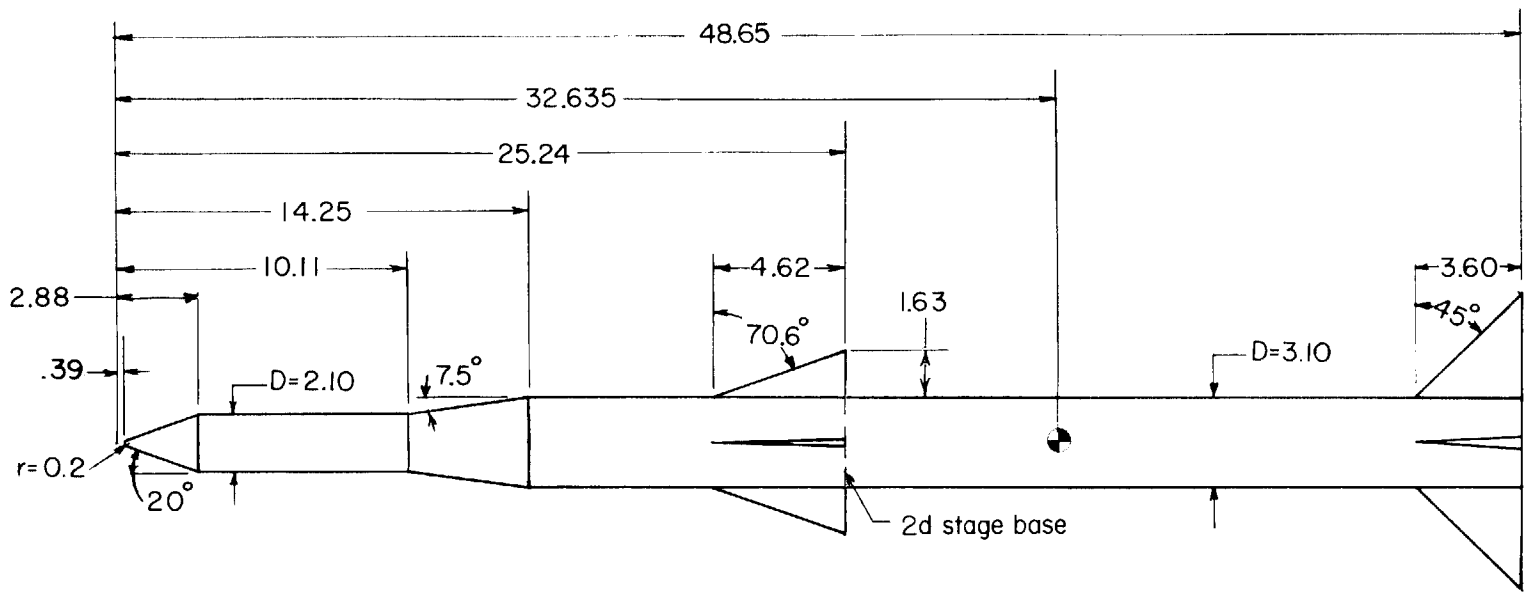

(a) Complete configuration.

Figure 1.- Model details. All dimensions are in inches unless otherwise noted.

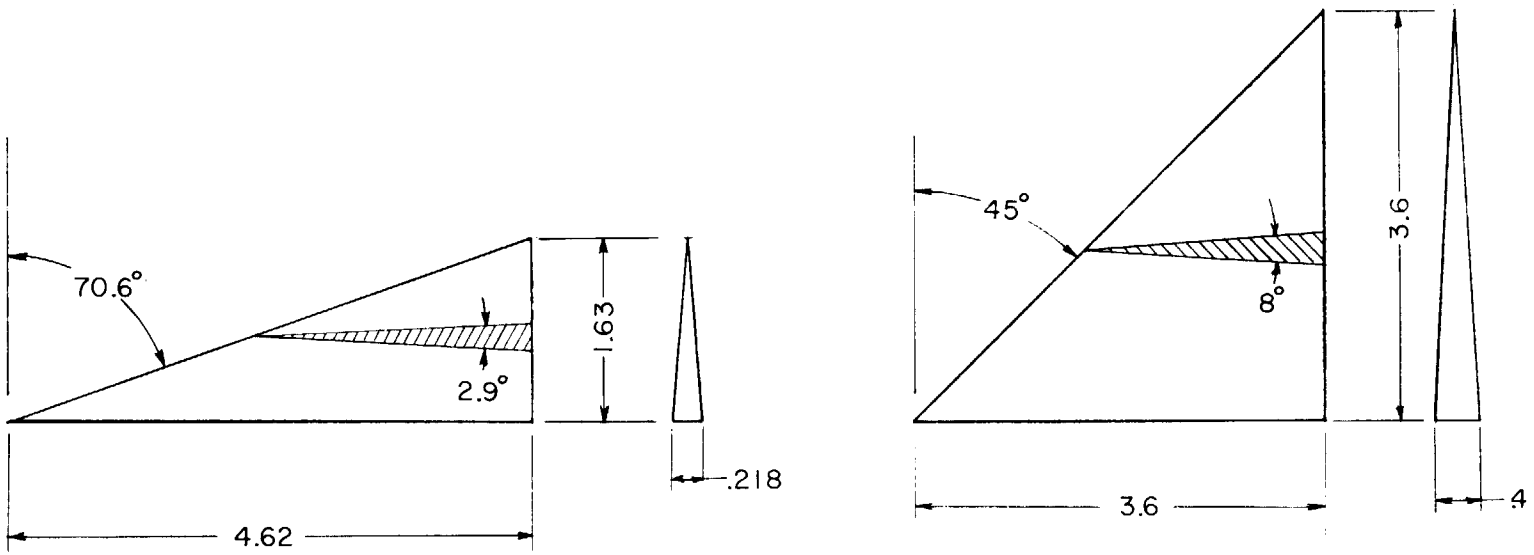

(b) Fin configurations.

Figure 1.- Concluded.

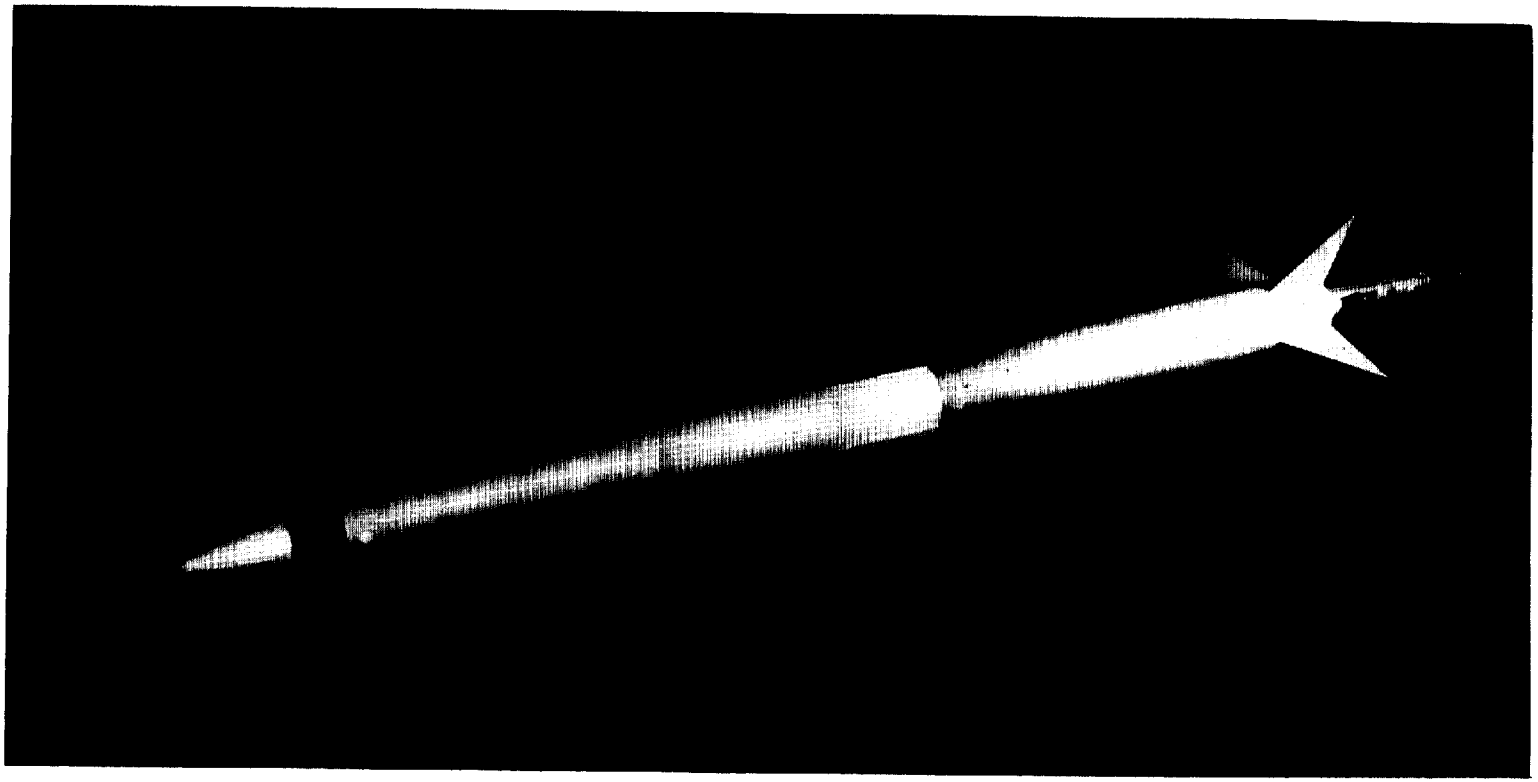

(a) Three-quarter front view.

L-60-2110

Figure 2.- Photographs of model used in the investigation.

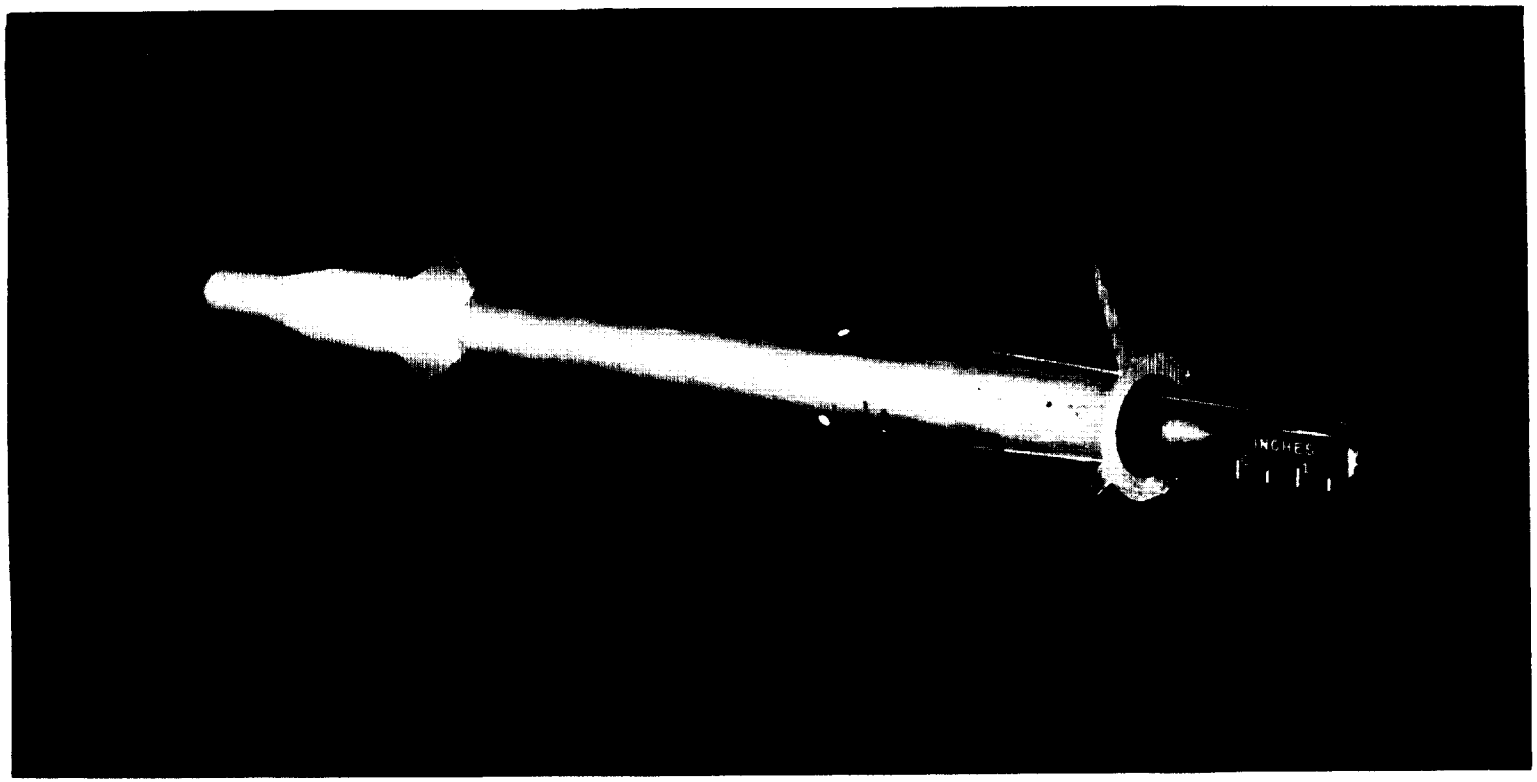

(b) Three-quarter rear view. L-60-2112

Figure 2.- Concluded.

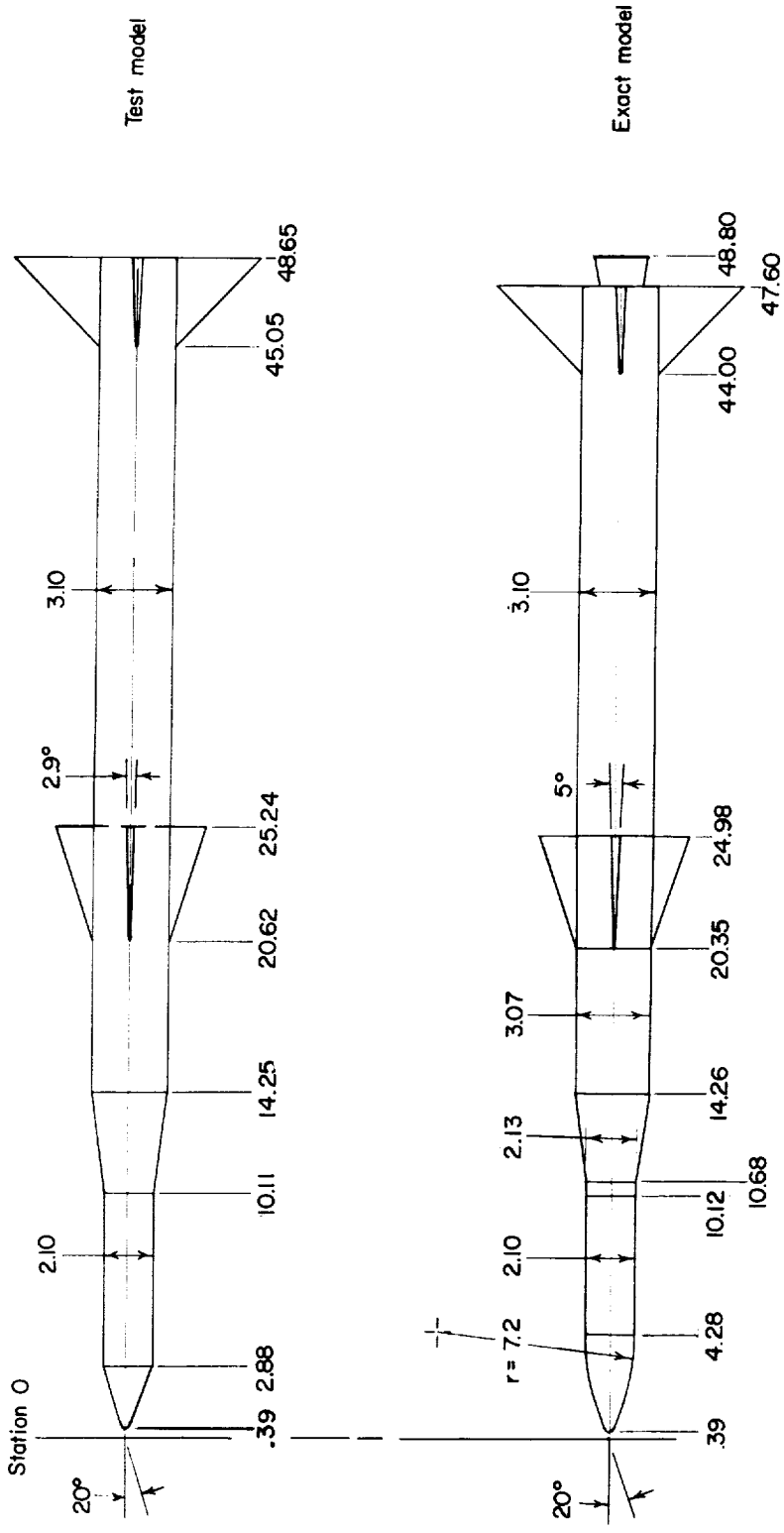

Figure 3.- Comparison of test model and early 1/10-scale model of Blue Scout Jr. Station locations shown are in inches unless otherwise noted.

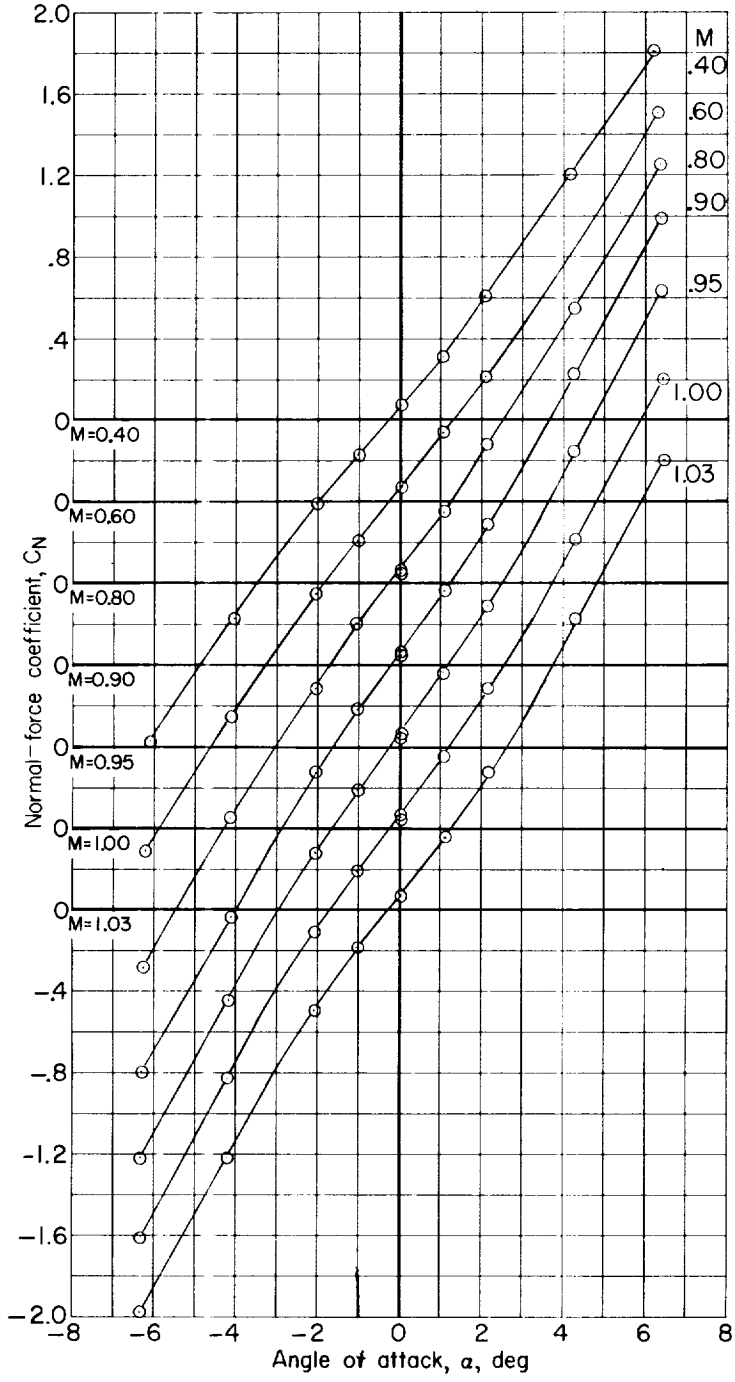

(a) Complete configuration.

Figure 4.- Variation of normal-force coefficient with angle of attack.

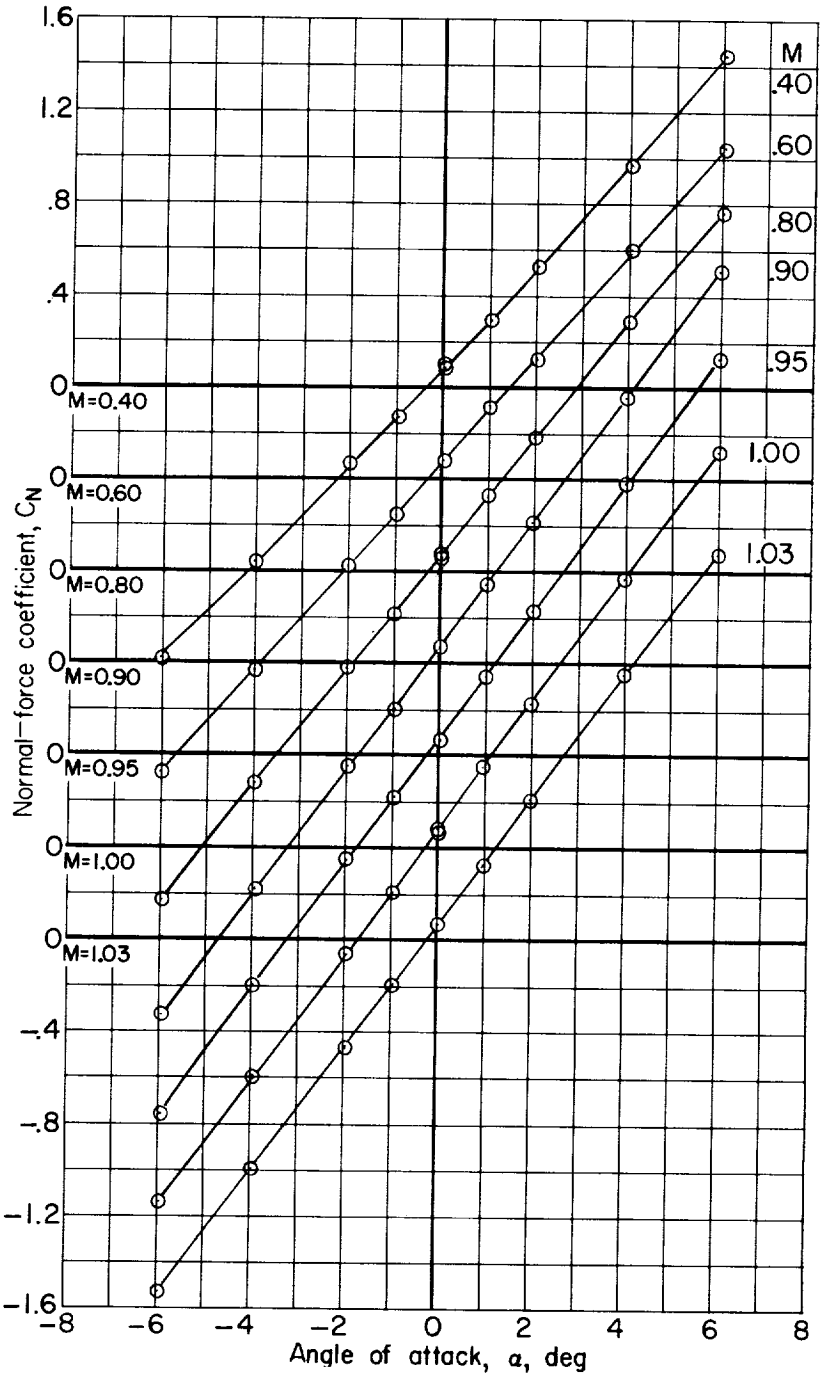

(b) Body plus rear fins.

Figure 4.- Continued.

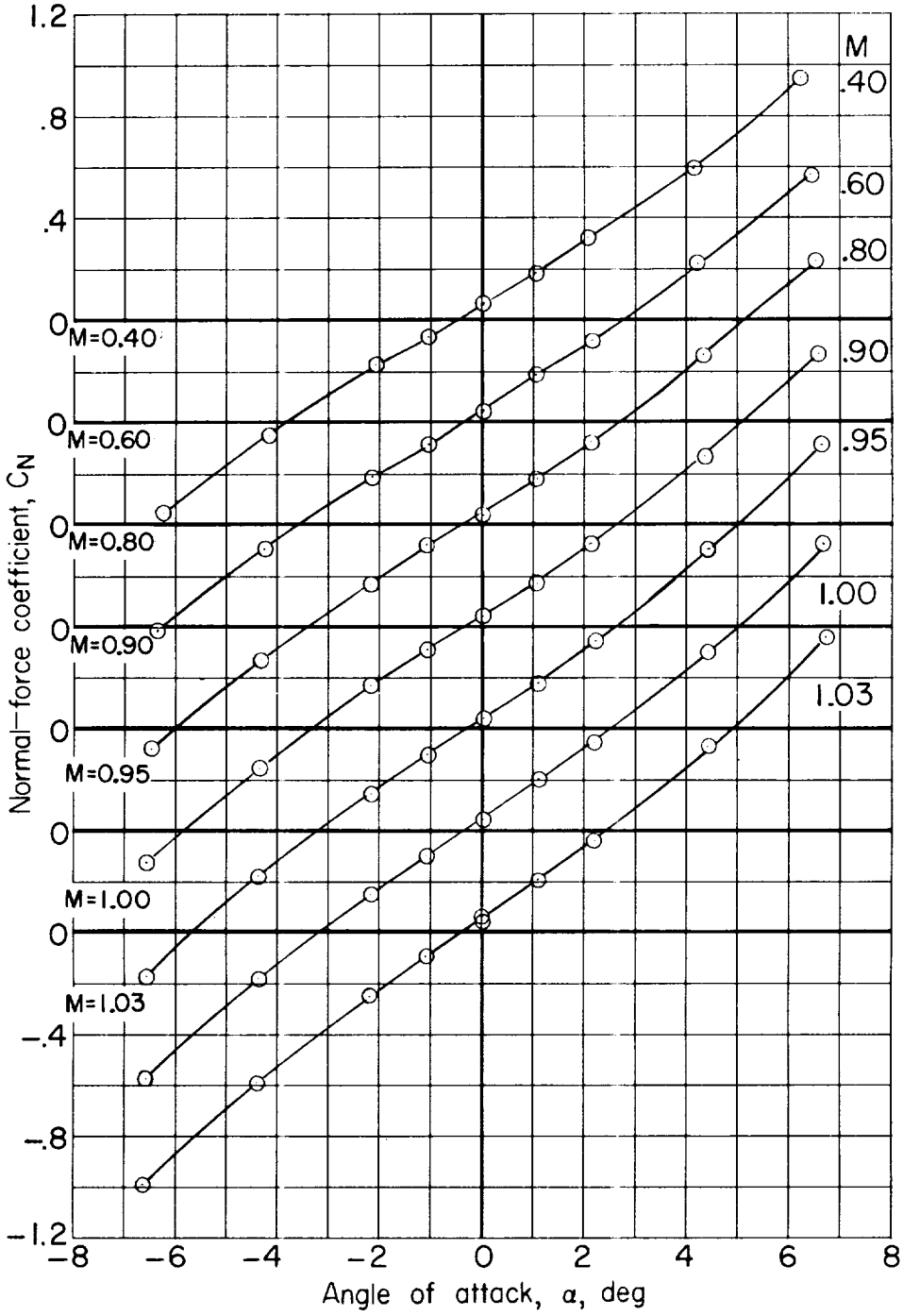

(c) Body plus forward fins.

Figure 4.- Continued.

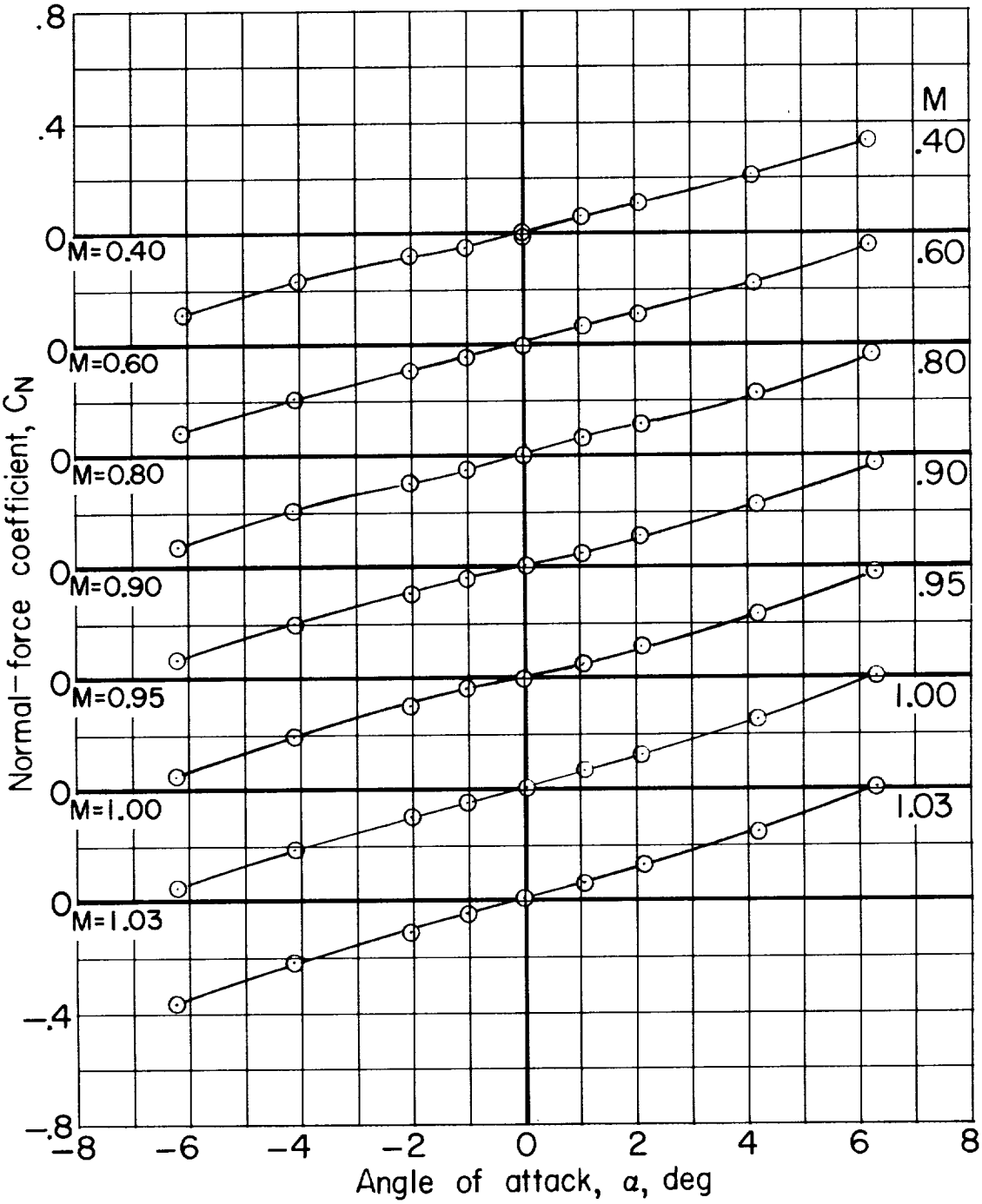

(d) Body alone.

Figure 4.- Concluded.

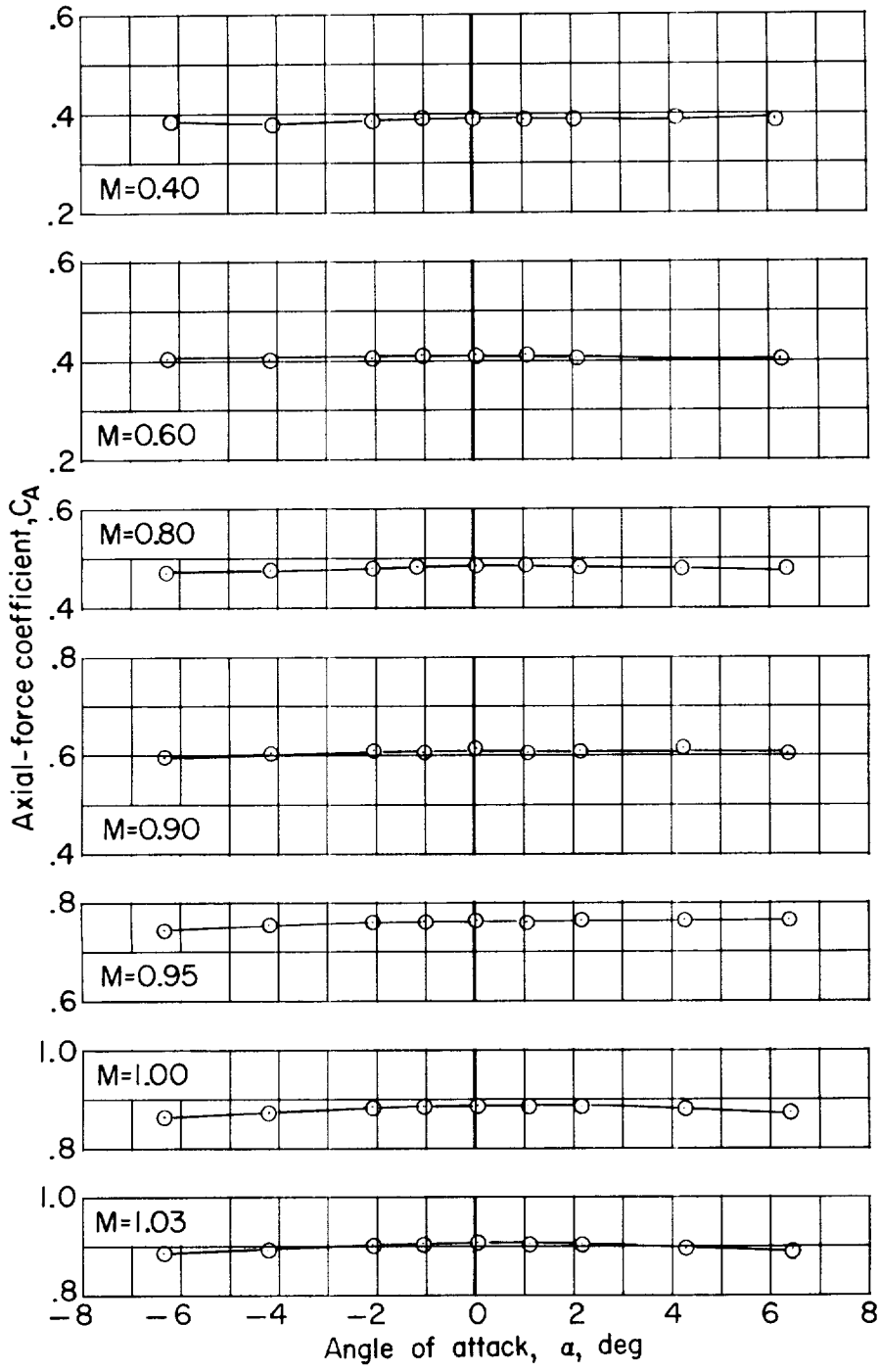

(a) C_A as a function of α for complete configuration.

Figure 5.- Variation of axial-force coefficient with angle of attack.

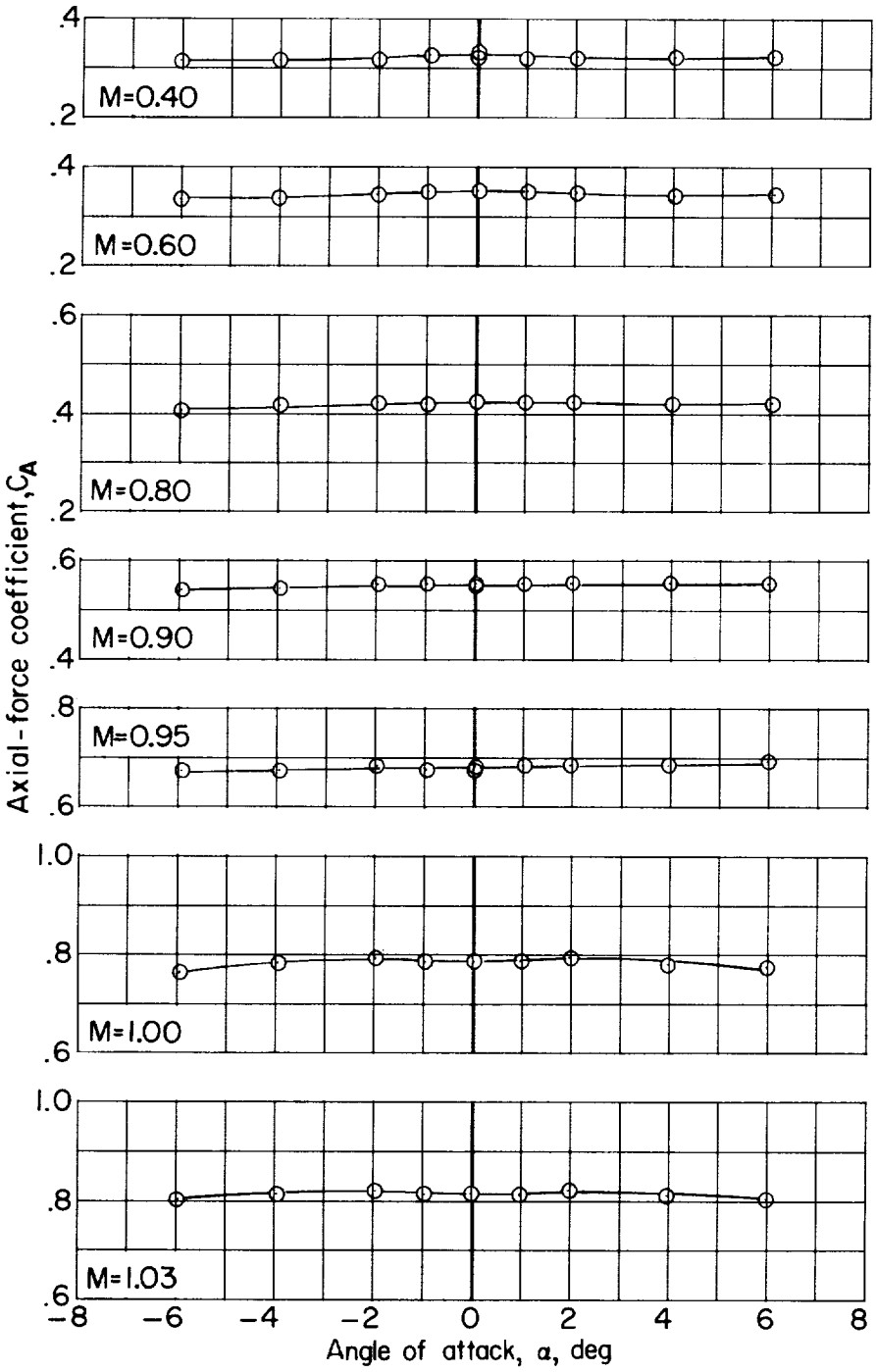

(b) C_A as a function of α for body plus rear fins.

Figure 5.- Continued.

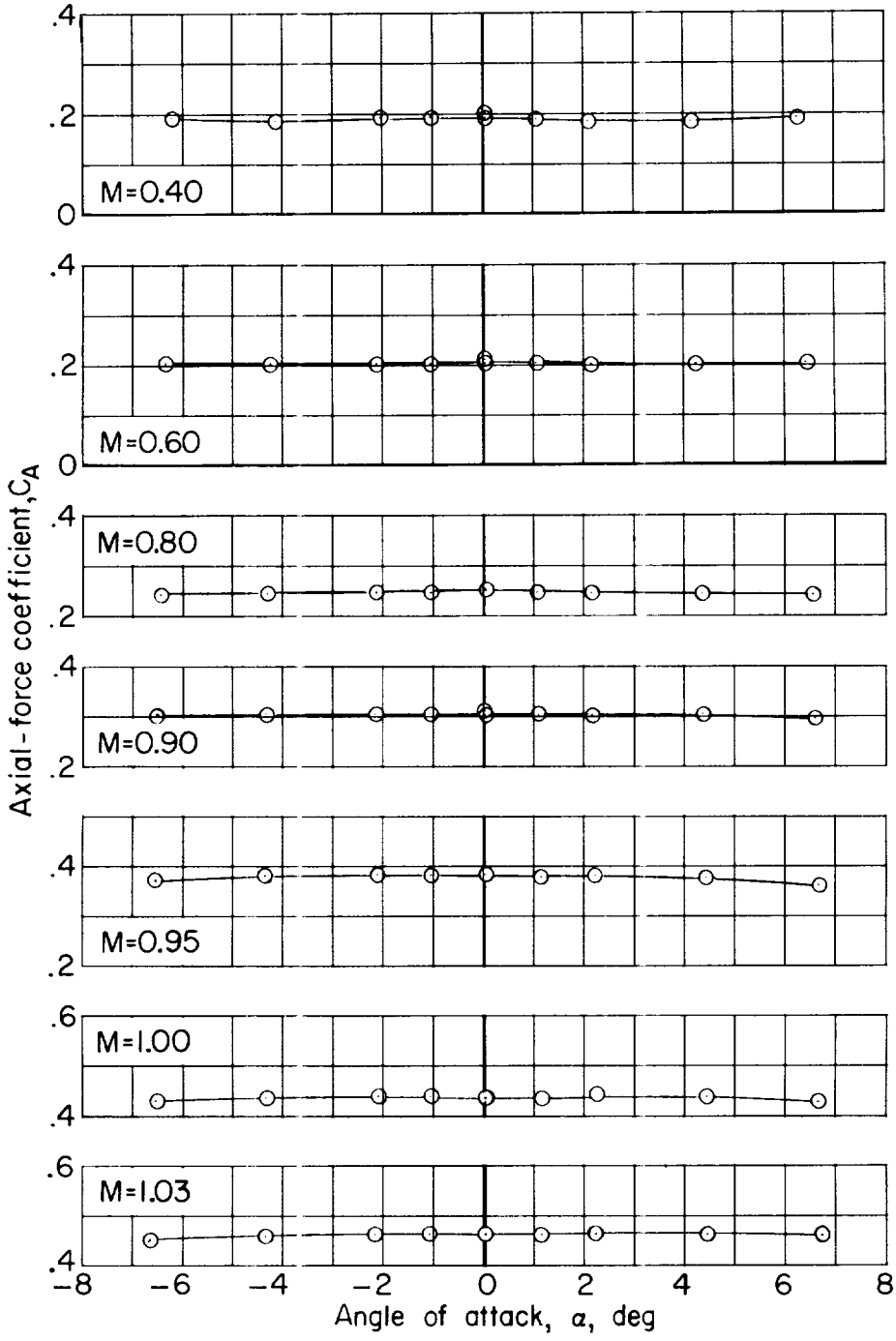

(c) C_A as a function of α for body plus forward fins.

Figure 5.- Continued.

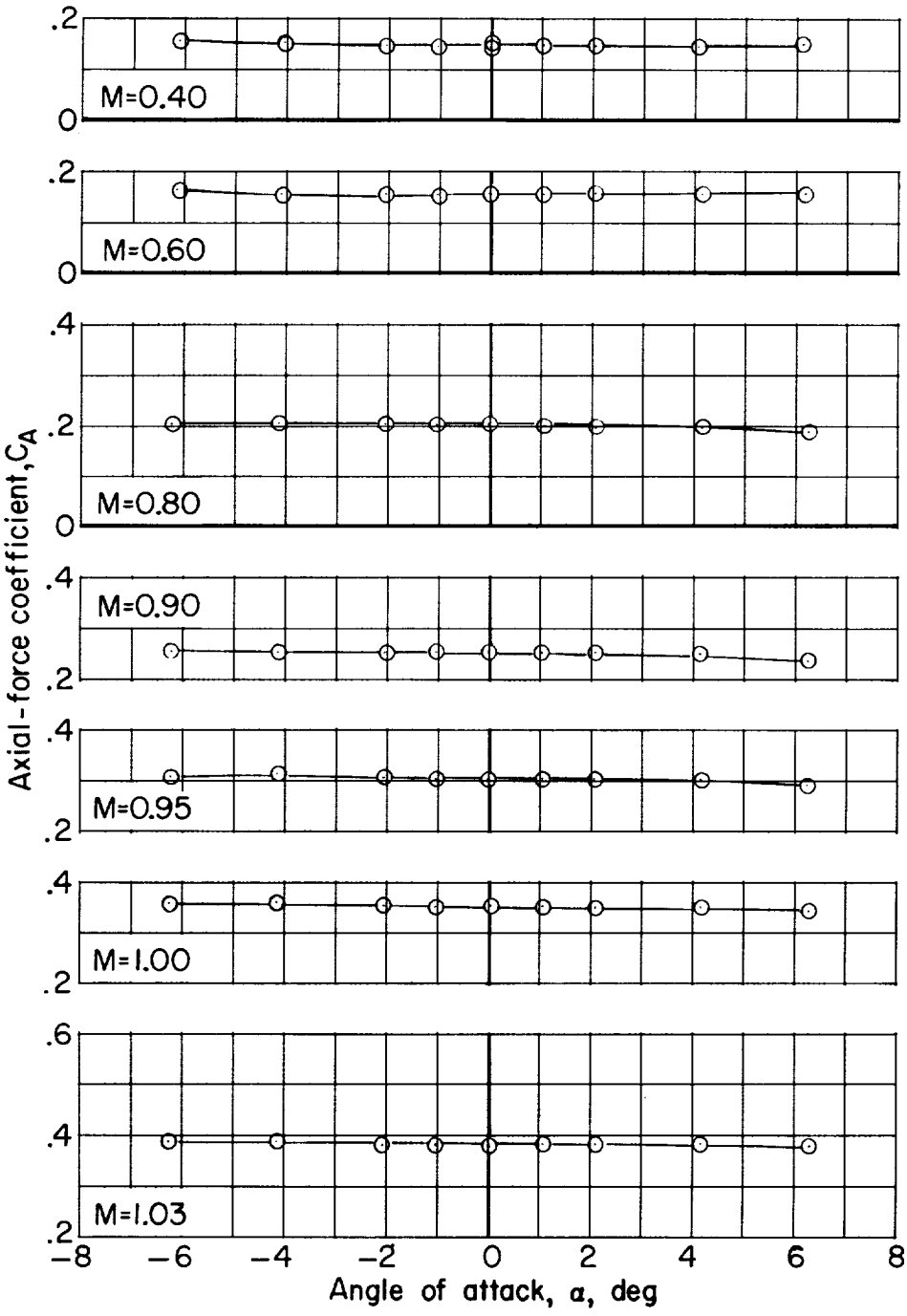

(d) C_A as a function of α for body alone.

Figure 5.- Continued.

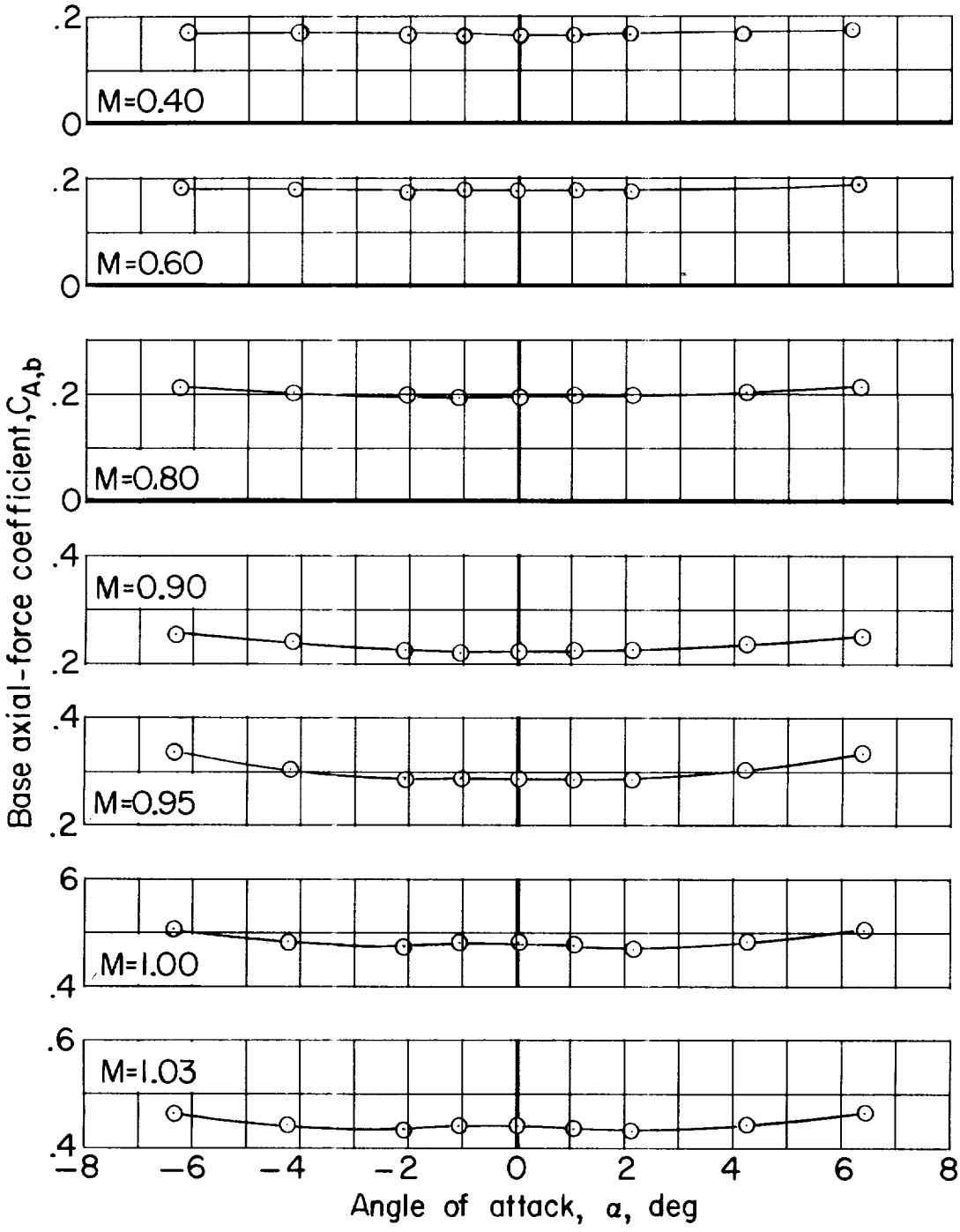

(e) $C_{A,b}$ as a function of α for complete configuration.

Figure 5.- Continued.

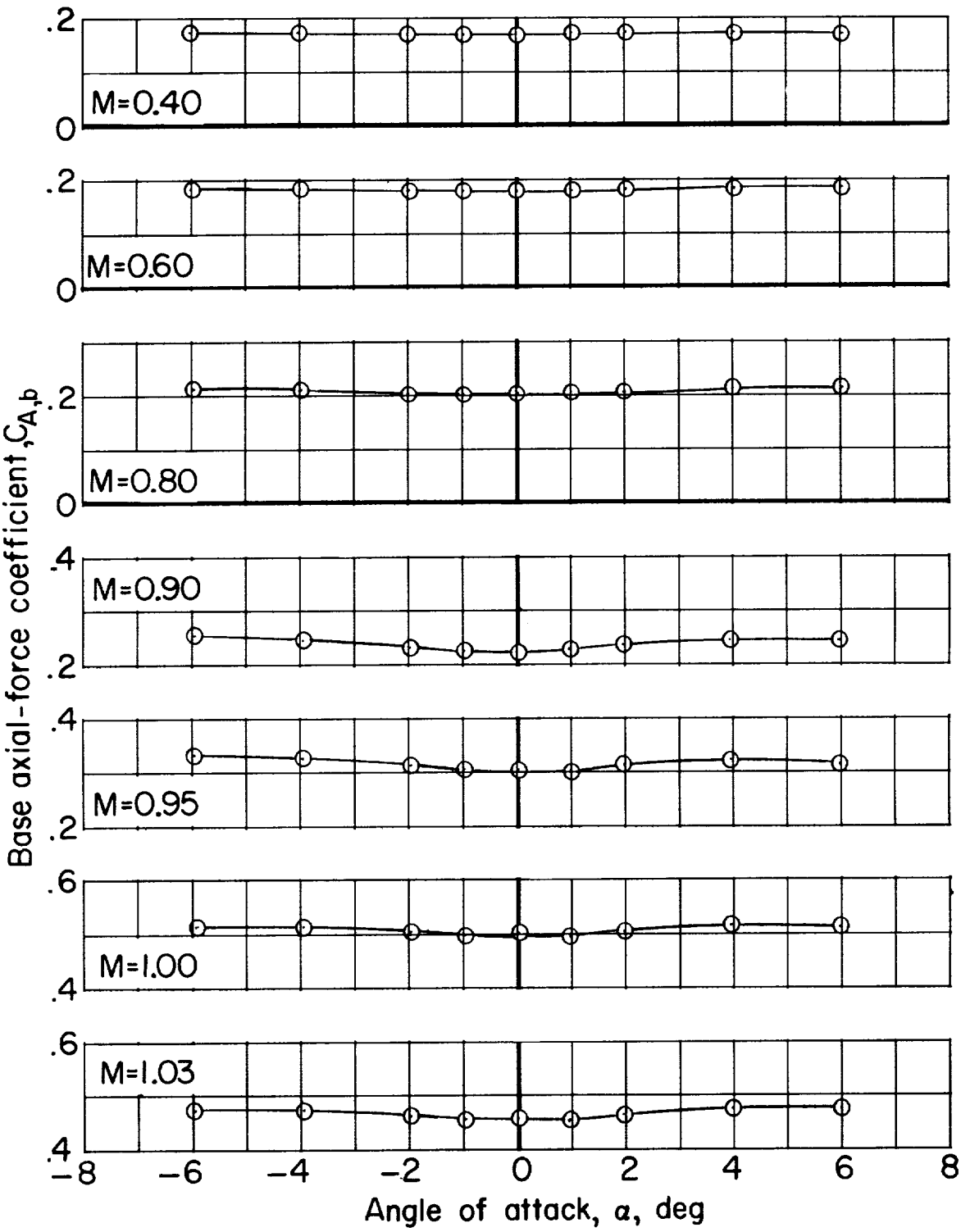

(f) $C_{A,b}$ as a function of α for body plus rear fins.

Figure 5.- Continued.

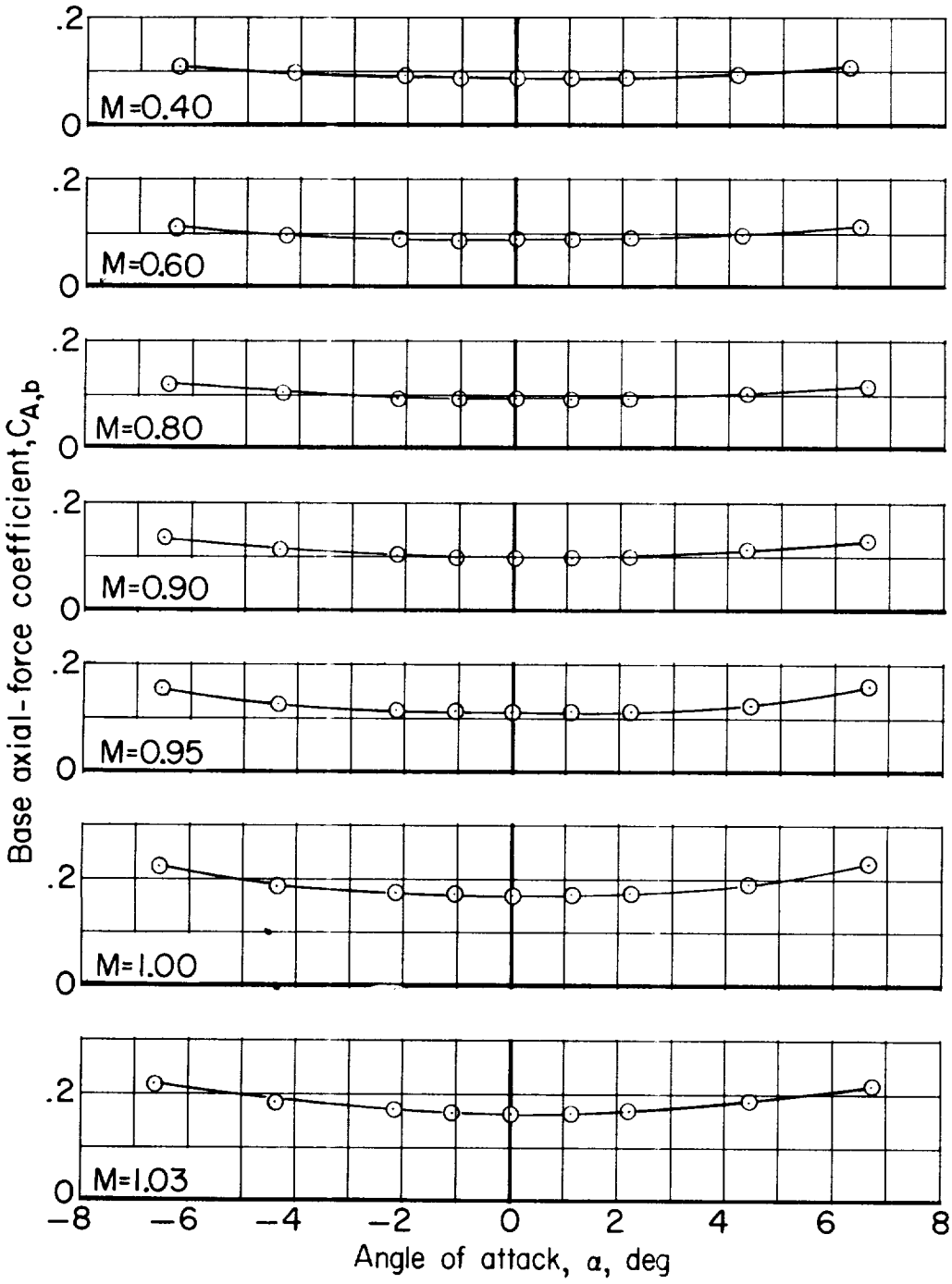

(g) $C_{A,b}$ as a function of α for body plus forward fins.

Figure 5.- Continued.

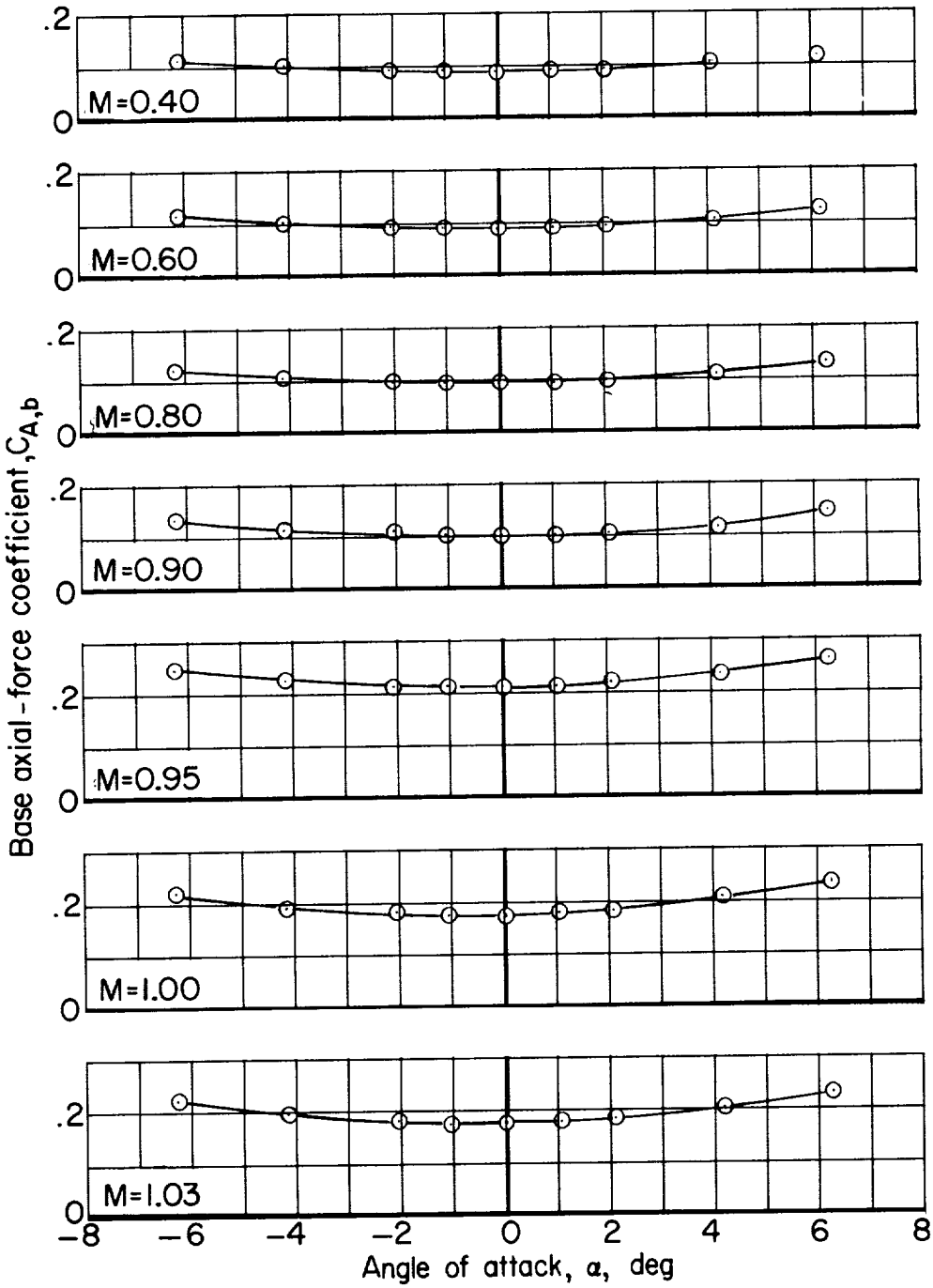

(h) $C_{A,b}$ as a function of α for body alone.

Figure 5.- Concluded.

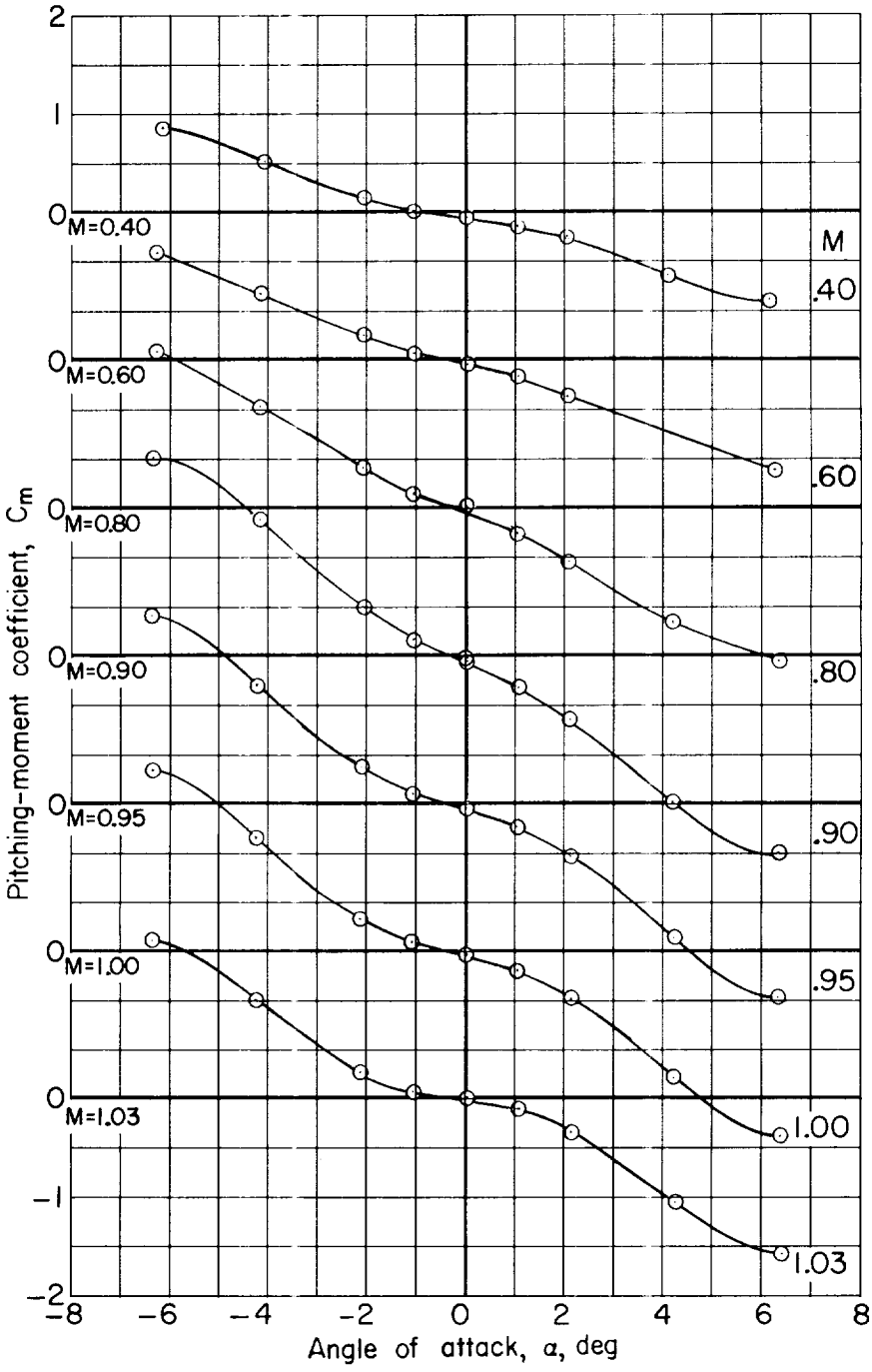

(a) Complete configuration.

Figure 6.- Variation of pitching-moment coefficient with angle of attack.

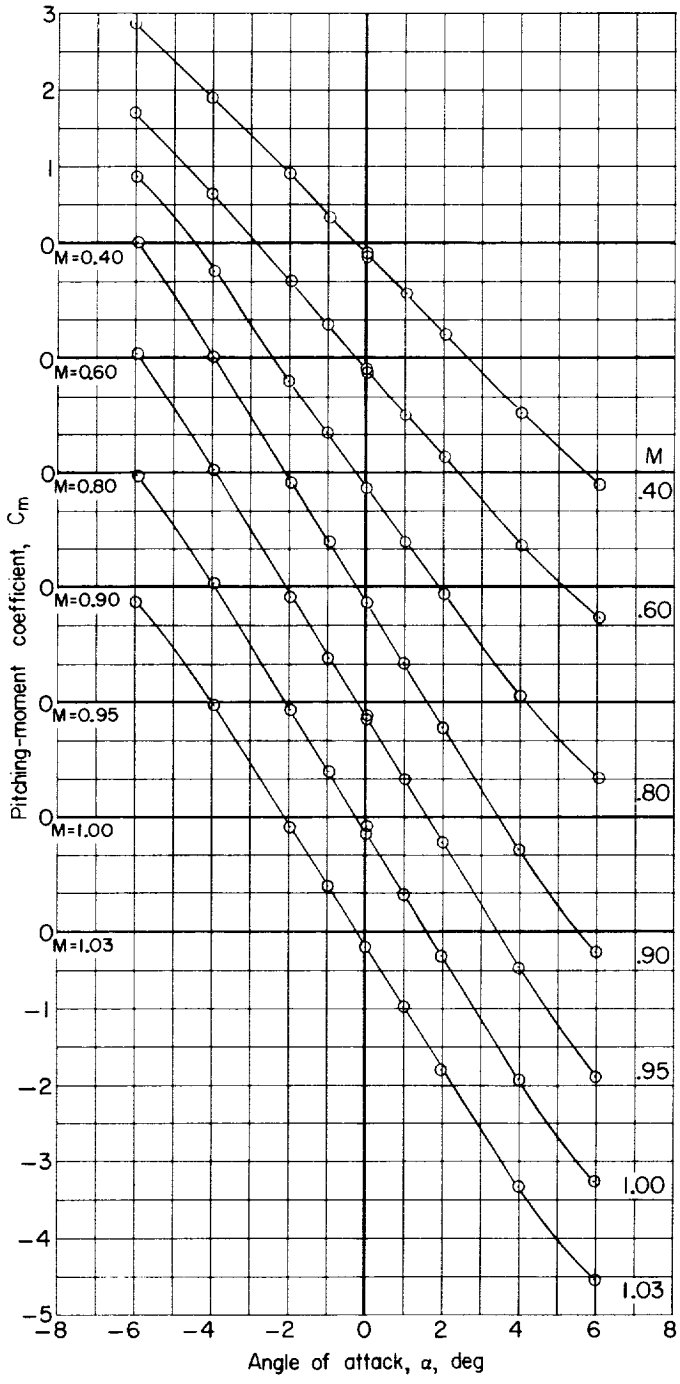

(b) Body plus rear fins.

Figure 6.- Continued.

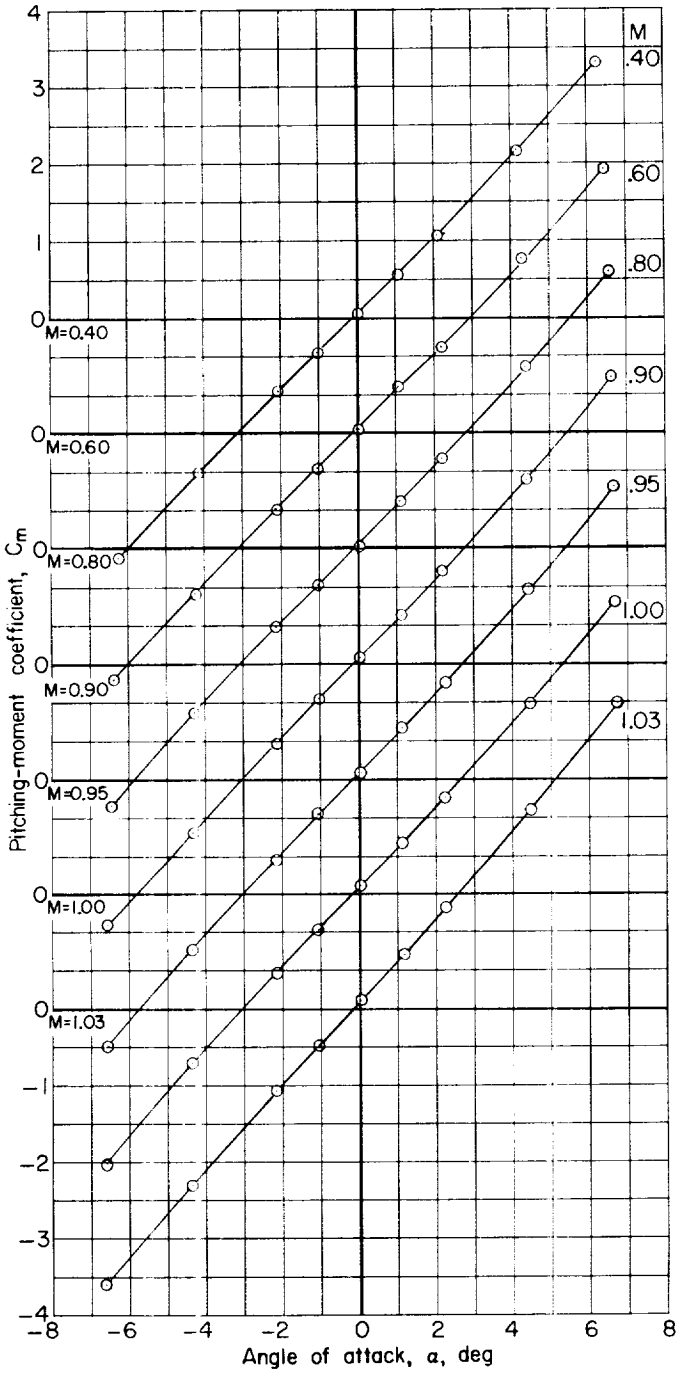

(c) Body plus forward fins.

Figure 6.- Continued.

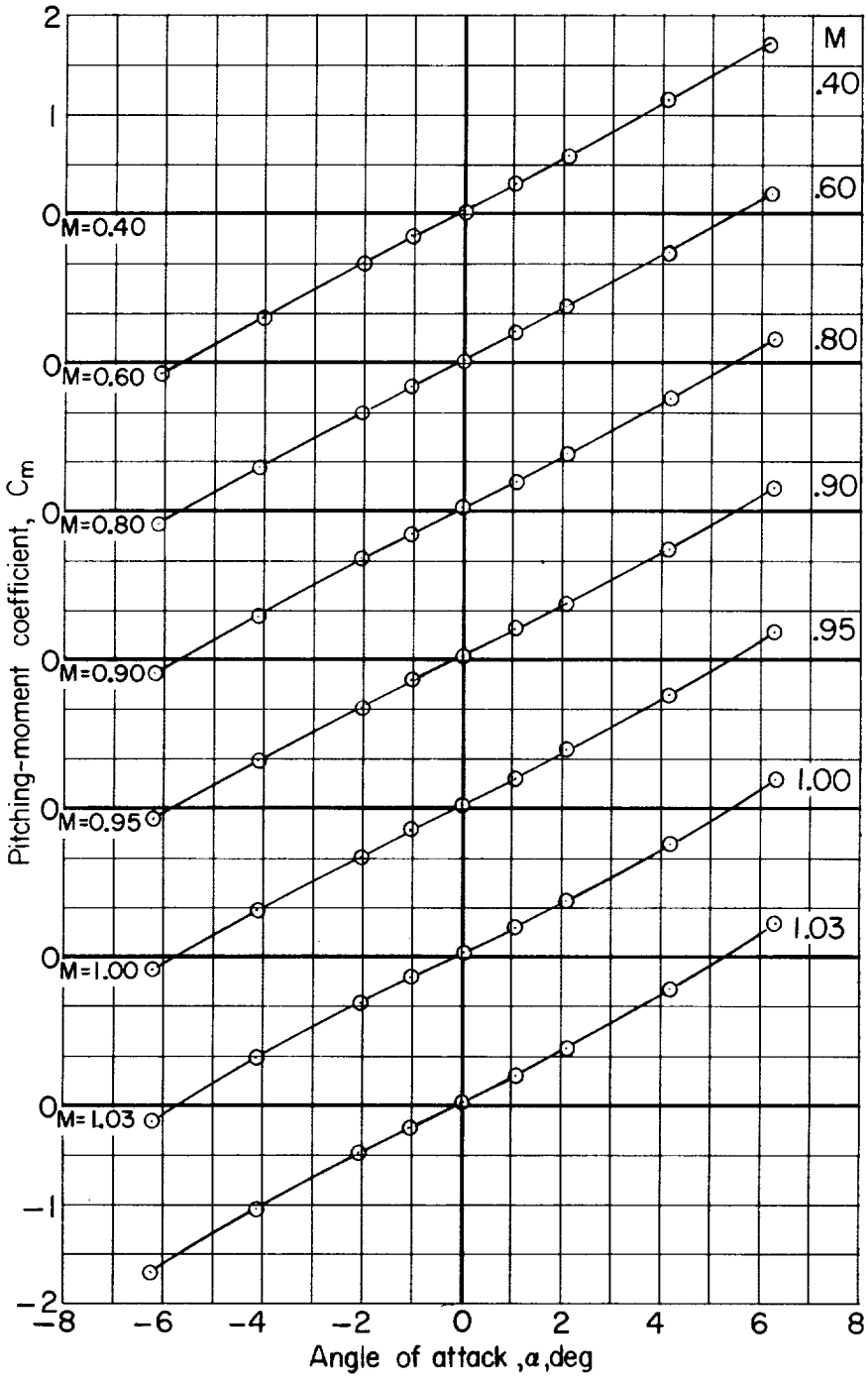

(d) Body alone.

Figure 6.- Concluded.

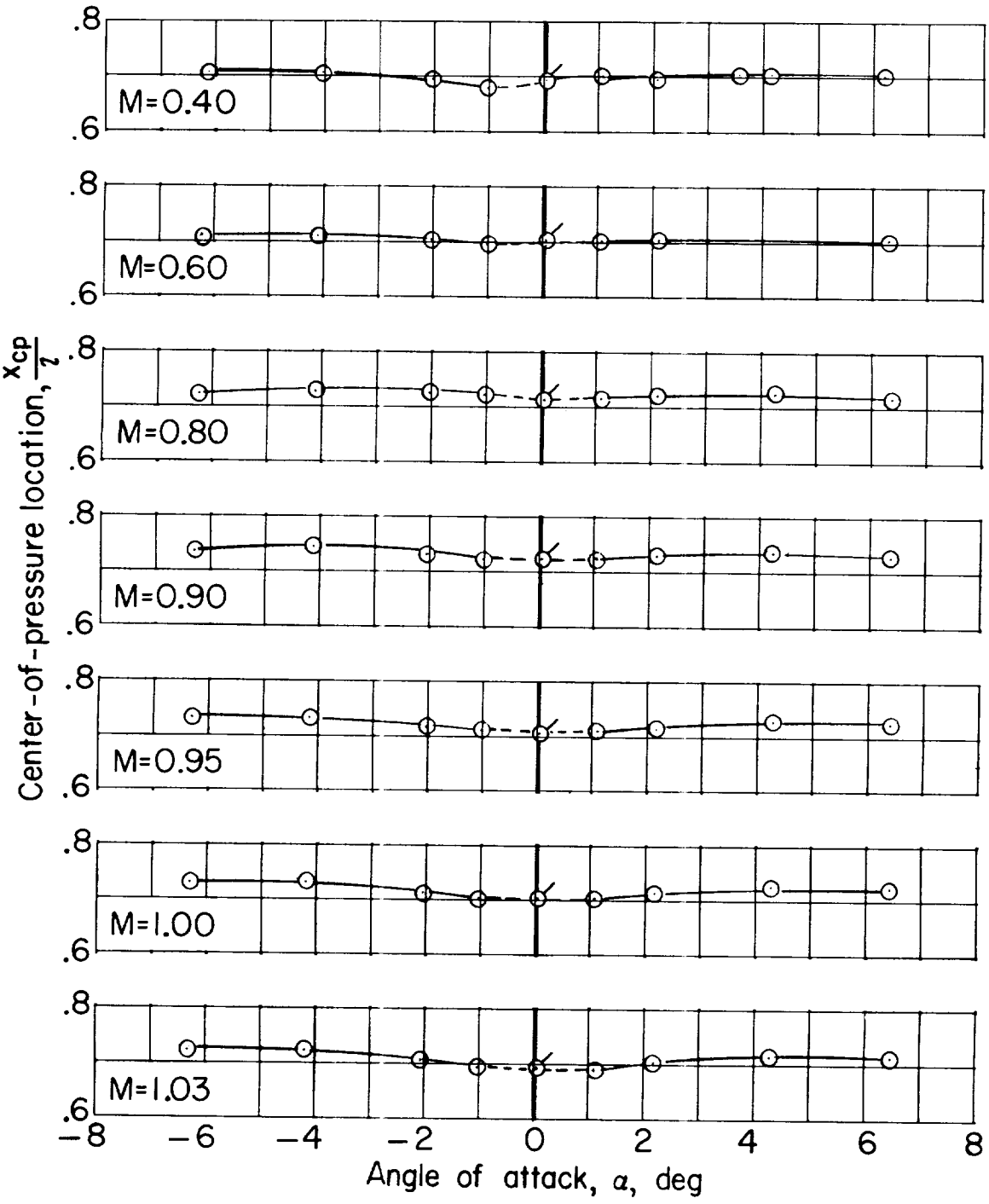

(a) Complete configuration.

Figure 7.- Variation of center-of-pressure location with angle of attack.

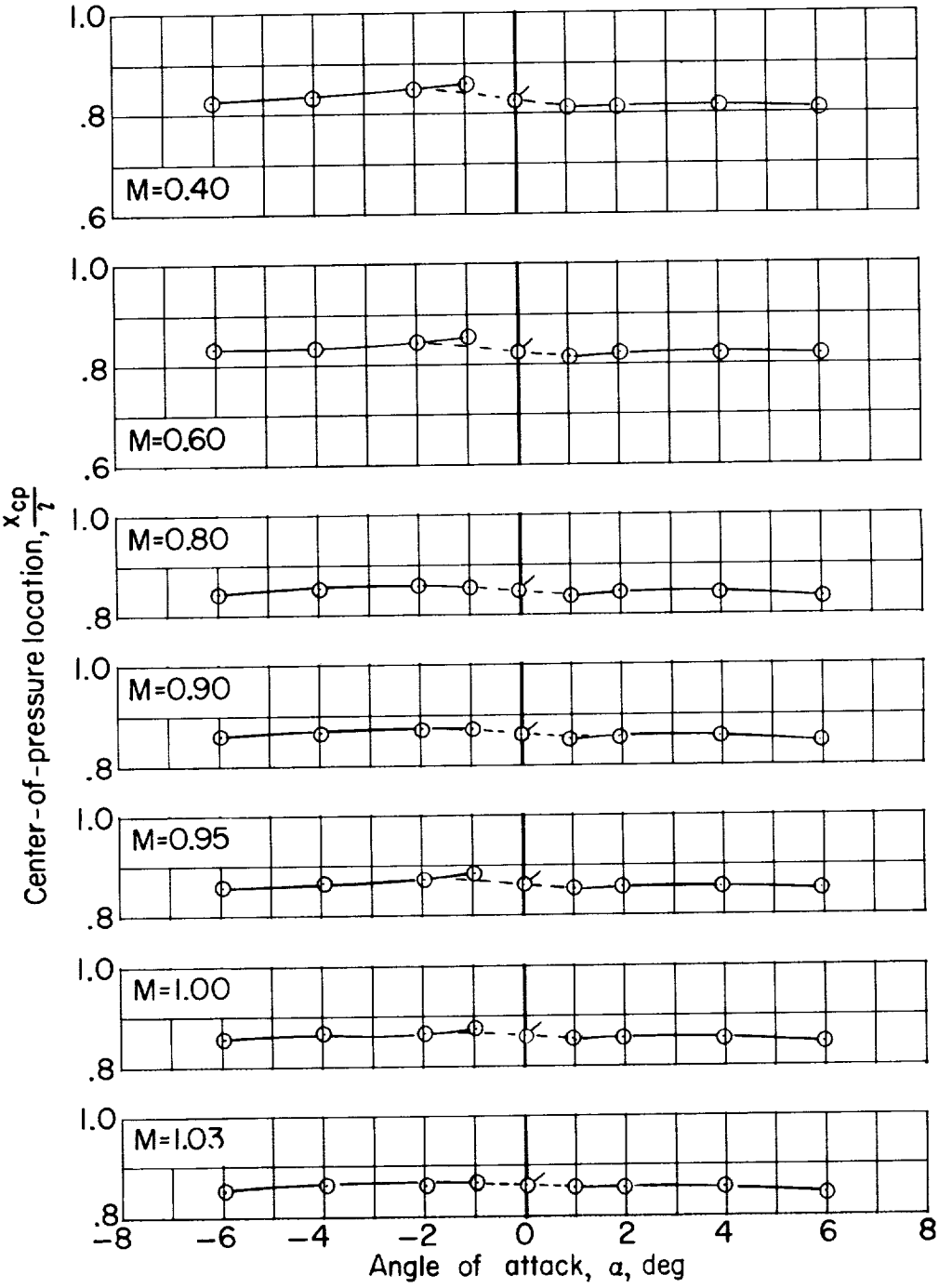

(b) Body plus rear fins.

Figure 7.- Continued.

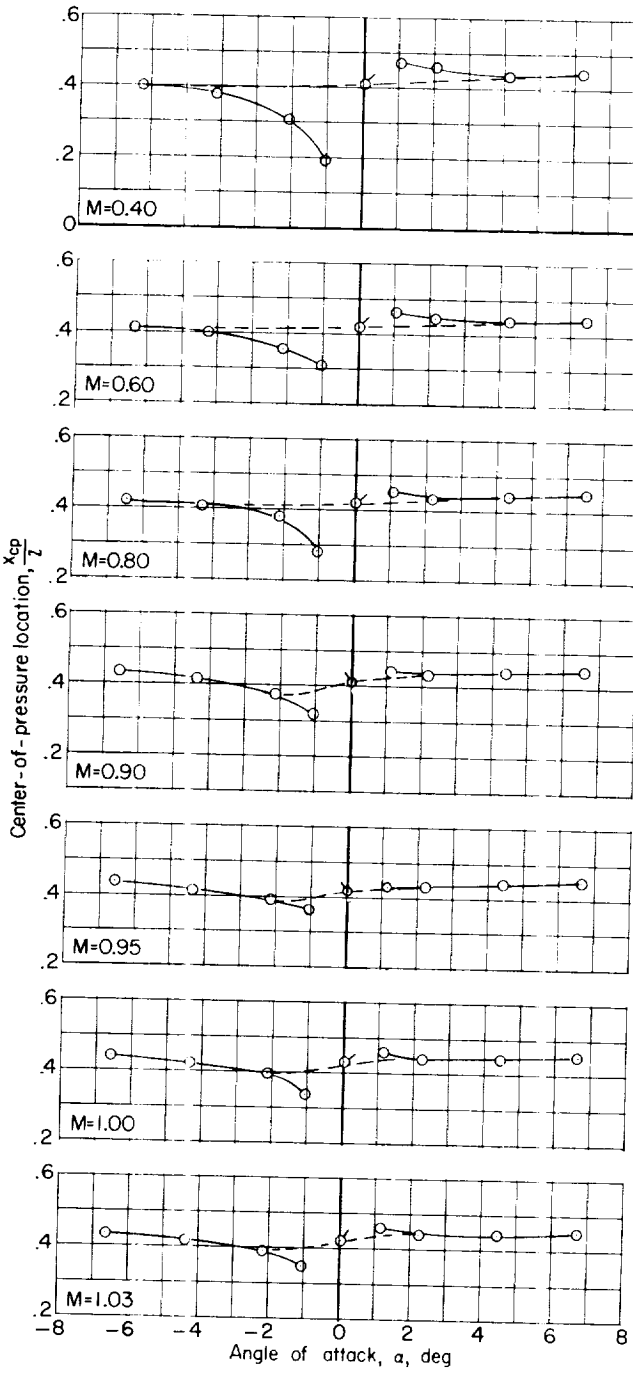

(c) Body plus forward fins.

Figure 7.- Continued.

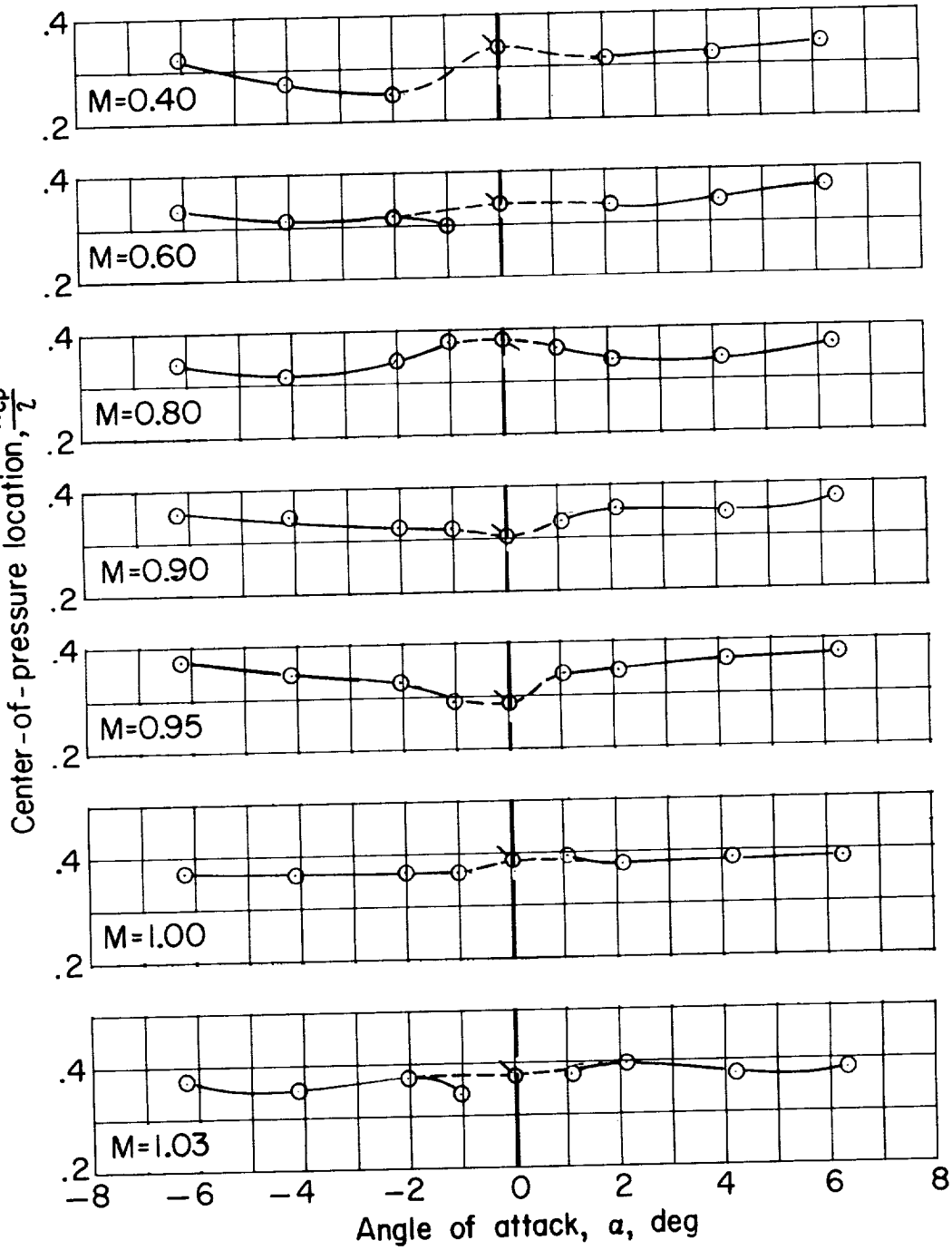

(d) Body alone.

Figure 7.- Concluded.

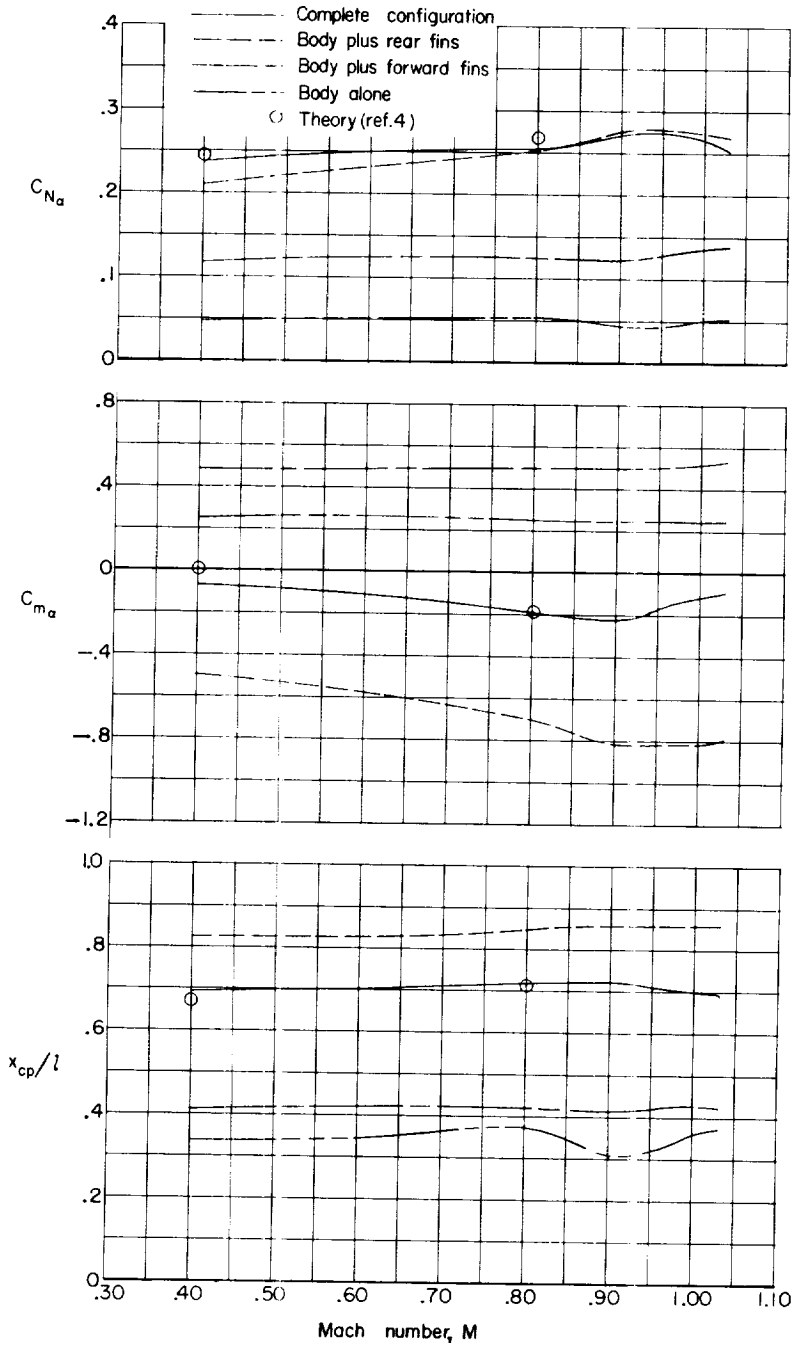

(a) C_{N_α}, C_{m_α}, and $\frac{x_{cp}}{l}$ as a function of Mach number.

Figure 8.- Summary of aerodynamic characteristics. $\alpha = 0^\circ$.

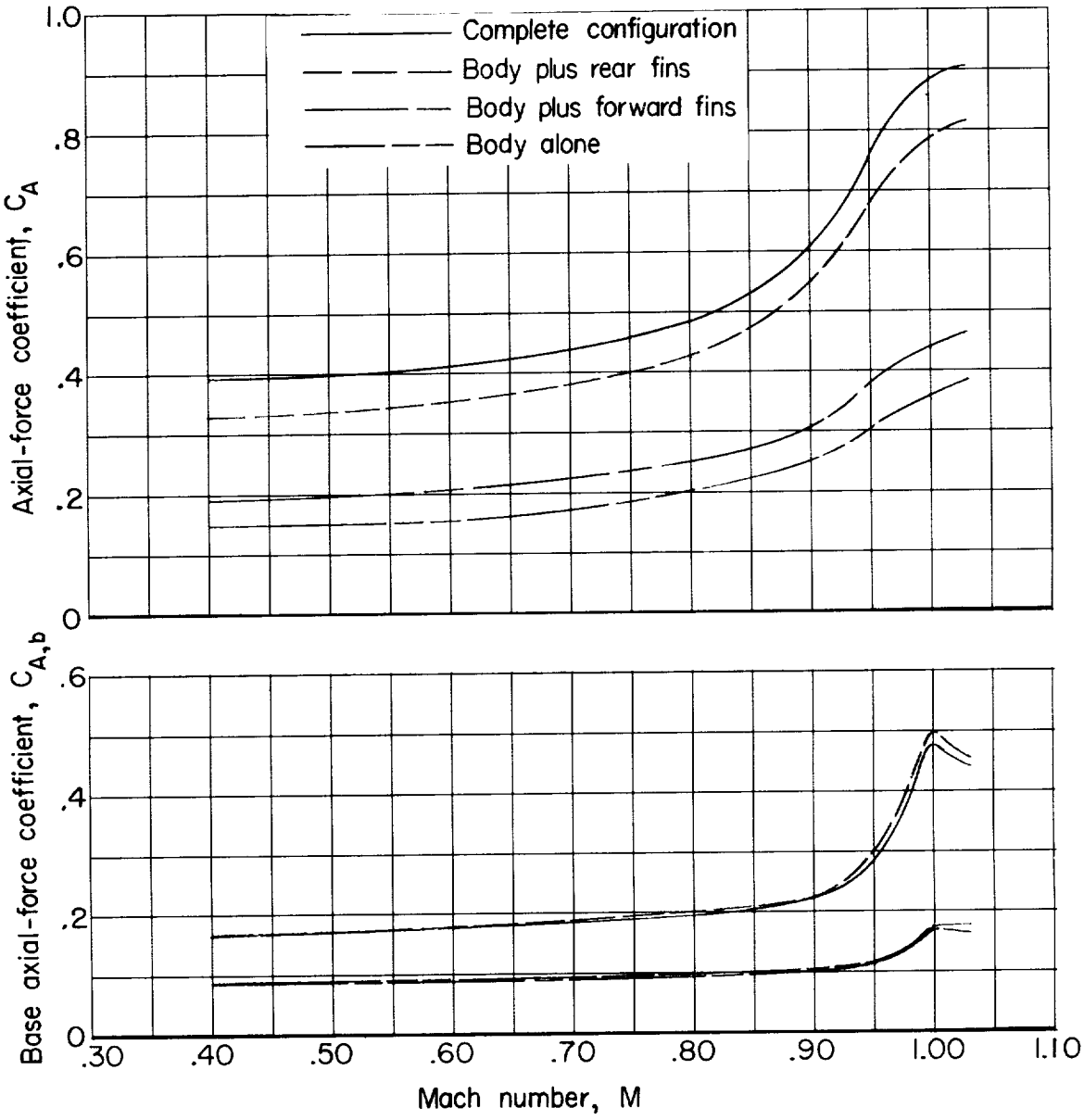

(b) C_A and $C_{A,b}$ as a function of Mach number.

Figure 8.- Concluded.